Green Chemistry

ROYAL SOCIETY OF CHEMISTRY

PAPER

View Article Online
View Journal | View Issue

Cite this: *Green Chem.*, 2020, **22**, 5123

Production of aromatics from biomass by computer-aided selection of the zeolite catalyst†

Vicente J. Margarit, Eva M. Gallego, Cecilia Paris, Mercedes Boronat, Manuel Moliner * and Avelino Corma *

Received 23rd March 2020,
Accepted 7th May 2020

DOI: 10.1039/d0gc01031f

rsc.li/greenchem

Taking into account that the transformation of biomass-derived 2,5-dimethylfuran (DMF) to *p*-xylene involves Diels–Alder (DA) cycloaddition as the limiting step, the use of an ITQ-2 zeolite obtained by direct synthesis (DS-ITQ-2) as a catalyst for this reaction is proposed based on the fact that the organic molecule employed for its synthesis mimics the size and shape of the DA oxanorbornene cycloadduct intermediate. Periodic Density Functional Theory (DFT) calculations reveal a better stabilization of the oxanorbornene intermediate within the external hemicavities or "cups" of the DS-ITQ-2 zeolite (MWW-framework) than in other zeolites employed for this reaction, such as FAU and Beta. Interestingly, experimental results also show improved catalytic conversion values for the DS-ITQ-2 zeolite compared to FAU and Beta, in good agreement with the stabilization energies calculated by DFT. The "*ab initio*" catalyst design presented here to enhance the catalytic performance for the transformation of biomass-derived products is a valuable example that could be employed for the rationalization of other chemical processes catalyzed by zeolites.

1. Introduction

The limited availability of fossil fuel reserves together with the increasing environmental and social concerns is imposing a gradual transition from fossil fuel-based technologies to more sustainable processes starting from renewable sources.[1] Biomass has received significant attention in the last few years as a renewable feedstock, mainly because a vast number of platform chemical molecules can be selectively produced from the primary biopolymers forming part of the lignocellulosic biomass.[2] A very interesting biomass-transformation route has been reported for the selective production of aromatic compounds, which is a challenging alternative to the current petroleum-based pathway.[3–5] The biomass-based path allows the yield towards the desired aromatic products to be maximised when the transformation occurs through consecutive reactions including a carbon–carbon cycloaddition followed by a dehydration reaction.[3]

From the different aromatic products, *p*-xylene is currently one of the most demanded chemicals, since it is considered a precursor of multiple polymers (*e.g.* polyester or polyethylene terephthalate, among others).[5–7] A renewable approach to obtain *p*-xylene is based on the tandem Diels–Alder (DA) cycloaddition between 2,5-dimethylfuran (DMF) and ethylene followed by the dehydration of the intermediate DA cycloadduct (see Fig. 1),[4,8] considering that both reactants can be achievable from biomass feedstocks.[9,10] When the recent literature is reviewed, the preferred catalysts reported for the selective transformation of DMF to *p*-xylene are large-pore zeolites, in particular FAU[4,11,12] and Beta-type zeolites.[13–17]

According to different experimental and computational studies, it has been established that the limiting step of the overall reaction is the non-catalyzed DA cycloaddition.[4,17,18] Thus, the ability to design zeolite-based catalysts that allow promotion of the DA reaction should have a direct influence on improving the overall reaction rates. Some authors have demonstrated that the inclusion of isolated Lewis acid sites in Beta zeolite enhances the DA reaction thanks to the preferential coordination of ethylene in the Lewis acid sites.[5,14,19]

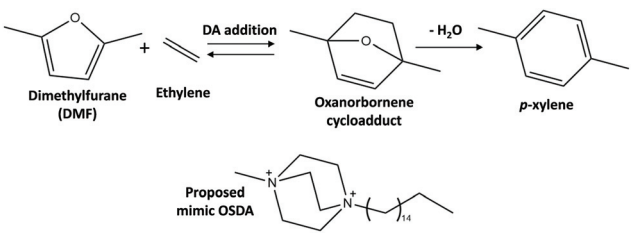

Fig. 1 Reaction scheme for the DA cycloaddition of dimethylfuran and ethylene followed by a dehydration reaction to obtain *p*-xylene (top), and the proposed mimic organic structure directing agent (bottom).

Instituto de Tecnología Química, Universitat Politècnica de València-Consejo Superior de Investigaciones Científicas, Avenida de los Naranjos s/n, 46022 València, Spain. E-mail: acorma@itq.upv.es, mmoliner@itq.upv.es

†Electronic supplementary information (ESI) available. See DOI: 10.1039/d0gc01031f

Alternatively, it has been described that the use of alkali-exchanged low-silica FAU zeolites, in particular KY, creates multi-site cooperative confined environments within the FAU cavities, which allow the DA reactivity to be increased by confining and stabilizing the reaction intermediates through interactions with extra-framework Lewis acids.[11,12,20]

Chemical reactivity in confined spaces is a matter of much interest.[21–23] In the case of zeolites, Derouane *et al.* introduced the role played by the van der Waals type of interactions and Pauli repulsion between the zeolite framework and the confined molecules within the zeolite pores and cavities.[21] We also presented that molecules in zeolites are confined at the molecular level and an electronic confinement can occur, the frontier orbitals of the molecule being strongly influenced when the pore diameter approaches the size of the molecule.[24] In fact, the aromaticity of anthracene in zeolites can be strongly disrupted due to the limitation of the molecular orbital spatial extension induced by the proximity of the pore walls.[24] The effect of zeolite confinement on transition state (TS) stabilization, and therefore, the effect on activity and selectivity for methanol carbonylation were shown by experimental and theoretical work.[25–27] Going one step further, it was presented that the confinement effect in zeolites could not only stabilize the transition states for several reactions, but also how this effect could be used for preparing organic structure directing agents (OSDAs) for an "*ab initio*" synthesis of zeolite catalysts for preselected reactions.[22,28,29]

The direct effect of the zeolite pore confinement for the Diels–Alder (DA) cyclodimerization of buta-1,3-diene to 4-vinylcyclohexene using large-pore zeolite catalysts and high reaction temperatures (250 °C) was reported by Dessau.[30] The catalytic role of zeolites in the DA reaction was explained on the basis of the concentrating effect of microporous materials. More recently, we have proposed that the DA reaction can be enhanced within the zeolite pores by the confinement effect due to the stabilization of the transition state by van der Waals and dispersion forces within the pores of the zeolite.[22,31] This was exemplified by the use of mimics of the transition states as OSDAs for zeolite synthesis,[28,29] allowing the preparation of a zeolite that enhances by an almost 3-fold increase the conversion for the DA cycloaddition between 1,3-cyclohexadiene and *N*-methylmaleimide with a pure silica large pore zeolite with the BEC structure.[31]

Since the transformation of DMF to *p*-xylene involves a DA cycloaddition as the limiting step, and the transition state and final product in DA reactions are very close, we have made use here of the concept of transition state mimics as OSDAs for this biomass-derived process, proposing an OSDA that could mimic the oxanorbornene cycloadduct intermediate (see Fig. 1). Indeed, we have recently shown that a surfactant-type 1,4-diazabicyclo[2.2.2]octane (DABCO)-derived molecule as shown in Fig. 1 is able to help in the one-pot synthesis (or direct synthesis, DS) of DS-ITQ-2,[32] which is a MWW-type zeolite with a large external surface area made by external hemicavities or "cups" in where the norbornene-type OSDA mimic could be stabilized.

MCM-22 (MWW structure) is composed of two independent pore systems, one defined by zig-zag 10-ring channels and another formed by 12-ring cavities that are only accessible through 10-ring windows, which make this material very interesting for very diverse catalytic applications.[33,34] In principle, the presence of large cavities in medium pore zeolites would allow the formation and stabilization of large intermediates, thus favoring the activity of reactions involving bulky transition states, as for instance those of the aromatic disproportionation reactions.[35,36] However, the formation of large products and by-products within the 12-ring cavities of MWW with limited diffusion paths through the 10-ring windows can limit the diffusion of the products out of the crystal and/or accelerate the MCM-22 deactivation.[35] To prevent this undesired fast deactivation, we proposed several years ago a new approach to achieve a 2-D zeolite with very thin layers of MWW following a surfactant-based swelling delamination process.[37] The resultant delaminated material, named ITQ-2, only exposes half of the 12-ring cavities at the external surface as "cups", where molecules can react and leave without the diffusion limitations along the closed cavities in MWW. The recent one-pot synthesis method of the highly delaminated DS-ITQ-2 material, which presents, on average, particles composed of 2–4 MWW-layers,[32] avoids the partial amorphization and dealumination produced during the synthesis of the delaminated ITQ-2.

Taking into account all of the above, we thought that the material synthesized by stabilization of the transition state mimic (oxanorbornene derived OSDA) should make a more adequate zeolite catalyst for the DA reaction between DMF and ethylene, due to the higher stabilization by confinement of the DA transition state. If this was so, we should expect a higher reaction rate for the DS-ITQ-2 than for the preferred Beta and FAU zeolite catalysts for this reaction.

We have carried out here a periodic DFT theoretical study that shows that the molecular confinement and stabilization of the oxanorbornene intermediate are higher in the hemicavities of MWW than in zeolite Beta and FAU. Experimentally, this higher stabilization leads to an improved catalytic activity for the one-pot synthesized DS-ITQ-2. In addition, the catalytic activity increases with the delamination degree of different DS-ITQ-2 samples, indicating that the larger the number of exposed hemicavities synthesized by decreasing MWW crystal size along the *c*-axis, the larger is the yield to the final aromatic product. These combined theoretical and experimental results provide a very valuable example demonstrating the importance of developing efficient "*ab initio*" catalyst designs to boost the catalytic performance of industrially relevant chemical processes.

2. Experimental

2.1. Computational details

Periodic density functional theory (DFT) calculations were performed with the VASP code[38] using the GGA-type functional of Perdew, Burke and Ernzerhof (PBE)[39,40] and the Grimme D2 method to take into account dispersion interactions.[41] The

valence density was expanded in a plane wave basis set with a kinetic energy cutoff of 600 eV, and the effect of the core electrons in the valence density was taken into account by means of the projected augmented wave (PAW) formalism.[42,43] Integration in the reciprocal space was carried out at the Γ *k*-point of the Brillouin zone. Electronic energies were converged to 10^{-6} eV and geometries were optimized by means of a conjugate-gradient algorithm until forces on atoms were less than 0.01 eV $Å^{-1}$. During geometry optimizations, the positions of all atoms in the system were allowed to relax without any restriction.

MWW crystallizes in a hexagonal *P*6/*mmm* space group with lattice parameters $a = b = 14.390$ and $c = 25.198$ Å, and contains 216 atoms in the conventional unit cell (72 Si and 144 O). A model for a delaminated ITQ-2 zeolite was created by hydrolyzing the two Si–O–Si bonds per unit cell linking the layers, and by expanding the lattice along *c* to a final value of $c = 35.216$ Å. Large hemi-cavities or "cups" (7.1 × 7.1 × 7.1 Å) are present on the external surface of MCM-22 and in the layers of the delaminated DS-ITQ-2 zeolites. FAU crystallizes in a cubic $Fd\bar{3}m$ space group with lattice parameters $a = b = c = 24.345$ Å, and contains large supercages of 11.2 Å diameter accessible through 12-ring windows. The unit cell used for the periodic calculations contains 576 atoms (192 Si and 384 O), and the reaction intermediate was always found at the center of the supercavity. The model used for BEA crystallizes in a tetragonal $P4_122$ space group with lattice parameters $a = b = 12.630$ and $c = 26.186$ Å, and contains 192 atoms (64 Si and 128 O) that form a three-dimensional 12-ring channel system.

2.2. Zeolite synthesis

Zeolites MCM-22[34] and DS-ITQ-2[32] have been prepared according to the procedures detailed in the literature. In particular, DS-ITQ-2_H was prepared by adding 12.82 g of double distilled water to 1.71 g of a 10 wt% aqueous solution of NaOH, followed by 0.14 g of sodium aluminate (Carlo Erba, 58.9% Al_2O_3, 38.7% Na_2O, 2.4% H_2O). Then, 1.12 g (2×10^{-3} mol) of 1-hexadecyl-4′-methyl-1,4-diazabicyclo[2.2.2]octane-1,4-diium ($C_{16}DC_1$), prepared according to the literature,[32] was added to the above mixture while stirring. After homogenization, 1.20 g of fumed silica (Sigma-Aldrich, particle size = 0.007 μm, 0.02 mol) and 0.595 g of hexamethyleneimine (HMI, Sigma-Aldrich, 6×10^{-3} mol) were added to the mixture and stirred vigorously for 1 h, obtaining a gel with the following molar composition: 0.15 Na_2O : 1 SiO_2 : 0.04 Al_2O_3 : 0.3 HMI : 0.1 $C_{16}DC_1$: 40 H_2O. The final gel was introduced into 35 mL PTFE lined stainless-steel autoclaves and heated at 150 °C for 7 days at 60 rpm. The solid was recovered by filtration, extensively washed with distilled water and dried at 100 °C overnight. DS-ITQ-2_L was prepared following the same procedure but adjusting the gel composition to 0.15 Na_2O : 1 SiO_2 : 0.04 Al_2O_3 : 0.3 HMI : 0.05 $C_{16}DC_1$: 40 H_2O. MCM-22 was prepared following the same procedure but adjusting the gel composition to 0.09 Na_2O : 1 SiO_2 : 0.04 Al_2O_3 : 0.5 HMI : 45 H_2O.

For comparison purposes, commercially available FAU (CBV720, Zeolyst) and Beta (CP811, Zeolyst) zeolites have also been considered.

The as-prepared samples were calcined at 560 °C for 6 hours to eliminate the OSDAs. Finally, the acid form of these materials was obtained by ion exchange of the calcined samples with 2.5 M NH_4Cl solution for 2 hours at 80 °C (liquid to solid ratio of 10), followed by a calcination treatment at 560 °C for three hours in air.

2.3. Characterization

Powder X-ray diffraction (PXRD) measurements were performed with a multisample Philips X'Pert diffractometer equipped with a graphite monochromator, operating at 40 kV and 35 mA, and using Cu Kα radiation ($\lambda = 0.1542$ nm).

Chemical analyses were carried out in a Varian 715-ES ICP-Optical Emission spectrometer, after solid dissolution in HNO_3/HCl/HF aqueous solution. Elemental analyses were performed by combustion analysis using a Eurovector EA 3000 CHNS analyzer.

The morphology of the samples was studied by field emission scanning electron microscopy (FE-SEM) using a ZEISS Ultra-55 microscope and by field emission transmission electron microscopy (TEM) using a JEM 2100F microscope. The delamination degree of the DS-ITQ-2 type materials has been estimated by a detailed inspection of 30 different TEM images and 275 different crystals for each material.

^{27}Al MAS NMR spectra were recorded at room temperature with a Bruker AV 400 MAS spectrometer at 104.2 MHz with a spinning rate of 10 kHz and 9° pulse length of 0.5 μs with a 1 s repetition time. The ^{27}Al chemical shift was referred to $Al^{3+}(H_2O)_6$.

2.4. Catalytic test

The catalytic experiments were performed in a commercial stirred high-pressure 50 ml Parr reactor. The catalysts were first activated within the reactor under a N_2 atmosphere at 300 °C for 3 h. After this, 20.6 g of a 0.5 M dimethylfuran (Sigma-Aldrich) solution in *n*-heptane (Sigma-Aldrich) was charged in the reactor, adjusting the reaction pressure to 52 bar with ethylene at 240 °C. Reaction samples were taken after 3 and 20 hours of reaction time, and the product analysis was performed by gas chromatography using dodecane (Sigma-Aldrich) as the internal standard. The composition was analyzed with a Varian CP-3800 GC equipped with a 30 m Carbowax column and a flame ionization detector. DMF and *p*-xylene were identified by comparing the retention times with standard chemicals. The concentration of the alkylated and condensed products was estimated by using the response factor (RF) for 1-methyl-4-propylbenzene and the additive RF of *p*-xylene and DMF, respectively, according to the literature.[14]

3. Results

3.1. Computational study

Considering that the limiting step for the Diels–Alder cycloaddition/dehydration reaction between DMF and ethylene to produce aromatics is the cycloaddition reaction between these two reactants,[13,14] and taking into account the geometrical

similarity between the transition state of the DA cycloaddition and the oxanorbornene product (see Fig. 2a), we have first performed a periodic DFT study of the stabilization by confinement of oxanorbornene at different positions within the voids of FAU, BEA and MWW zeolites. BEA and FAU zeolites have both been described in the literature as the active catalysts for selectively achieving *p*-xylene from biomass-derived furanes.[4,13–16] Thus, the stabilization of the reaction intermediate, oxanorbornene, has been explored at different positions within the FAU and BEA structures, and the best geometrical fitting has been obtained in the middle of the supercavity in the case of FAU (see Fig. 2b) and at the channel intersection in the BEA structure (see Fig. 2c). The calculated values for the stabilization energies of the reaction intermediate were −12.0 and −15.7 kcal mol^{-1} for FAU and BEA, respectively. From these results, one could expect that the higher stabilization offered by the Beta zeolite should facilitate the limiting-step DA cycloaddition reaction thanks to the better confinement of the oxanorbornene intermediate within the Beta micropores.

Taking into account that the direct synthesis of the delaminated MWW material, DS-ITQ-2, has been achieved using a surfactant template where its cationic head, 1,4-diazabicyclo [2.2.2]octane (DABCO), is placed within the external "cups",[32] and the similarity in size and shape between the oxanorbornene intermediate and DABCO, the OSDA mimic concept could be applied here for the biomass-derived DA cycloaddition/dehydration reaction considering the external "cups" of the MWW structure as potential ideal carriers to favor the DA cycloaddition reaction between DMF and ethylene. Thus, the stabilization energy of oxanorbornene has been calculated in the external "cups" of the MWW structure (see Fig. 2d), achieving a value of −19.6 kcal mol^{-1}, which is remarkably higher compared to the values calculated for Beta and FAU zeolites (−15.7 and −12.0 kcal mol^{-1}, respectively).

According to the DFT calculations, the highly accessible external "cups" in the MWW-structure would be able to stabilize the norbornene-type transition state better than other previously reported zeolites, such as Beta and FAU.

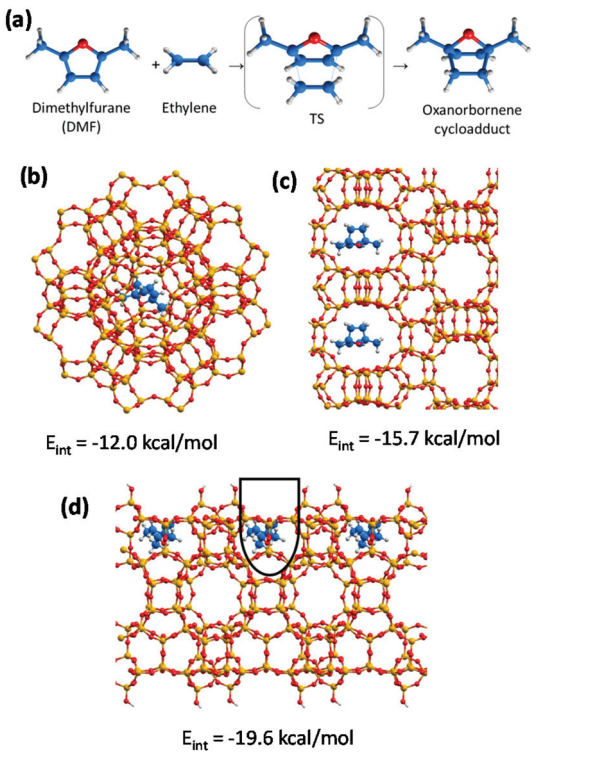

Fig. 2 Optimized structures of the Diels–Alder reactants, transition state and intermediate (a) and of the oxanorbornene intermediate in the cavities of FAU (b), pores of BEA (c) and external hemicavities of MWW (d). C, O, Si and H atoms are depicted as blue, red, yellow and white balls.

3.2. Synthesis and characterization of the MWW-type zeolites

The one-pot synthesis of a highly delaminated MWW-type structure, DS-ITQ-2, has been recently achieved by using a surfactant-type DABCO-derived molecule, whose structure is very similar to that of the oxanorbornene molecule described as the intermediate of the DA reaction between DMF and ethylene (see Fig. 1). Since the DABCO-derived cationic head has been described as the appropriate template to stabilize the external hemicavities or "cups" of the MWW structure, the preparation of two DS-ITQ-2 materials with different delamination degrees has been attempted by modifying the amount of the DABCO-type surfactant in the synthesis gel.[32] Two DABCO-surfactant/Si molar ratios have been considered, 0.05 and 0.1, for the one-pot synthesis of the DS-ITQ-2 materials (see the Experimental section for details). Previous studies have shown that the optimized Si/Al molar ratio to prepare the one-pot highly delaminated DS-ITQ-2 sample was ~12.[32]

The PXRD patterns of the resultant solids show the presence of the characteristic peaks of the DS-ITQ-2 structure (see Fig. 3). The differences within their PXRD patterns, where the sample prepared with a larger amount of surfactant, DS-ITQ-2_H, shows broader and less intense peaks, would suggest a different number of layers and, therefore, different dimensions of the crystals along the *c*-axes, with the corresponding different number of exposed hemicavities. Indeed, FE-SEM images of both DS-ITQ-2 samples indicate the formation of very thin platelet crystals with layer dimensions of ~150–200 nm along the *a*–*b* axes (see DS-ITQ-2_L and DS-ITQ-2_H in Fig. 4). Nevertheless, it seems that the DS-ITQ-2_H sample presents a larger proportion of these thin platelet crystals compared to DS-ITQ-2_L (see Fig. 4). This experimental observation would agree with the higher delamination nature achieved within DS-ITQ-2_H, as PXRD patterns suggested. To unravel the different delamination nature between DS-ITQ-2_H and DS-ITQ-2_L, these two samples have been characterized by HRTEM to estimate the thickness distribution of the final thin platelet crystallites (see Fig. 5). A systematic evaluation of many HRTEM images confirms that the DS-ITQ-2_H sample presents a larger amount of crystallites formed by one and two MWW-layers (~75%, see Fig. 6) than the DS-ITQ-2_L sample (below 60%, see Fig. 6).

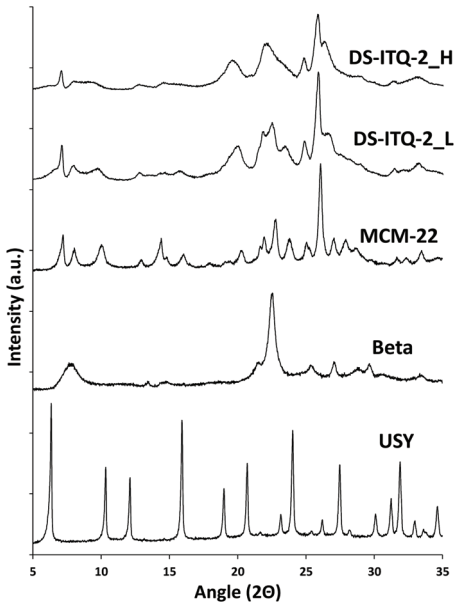

Fig. 3 PXRD patterns of the different zeolites employed in this study.

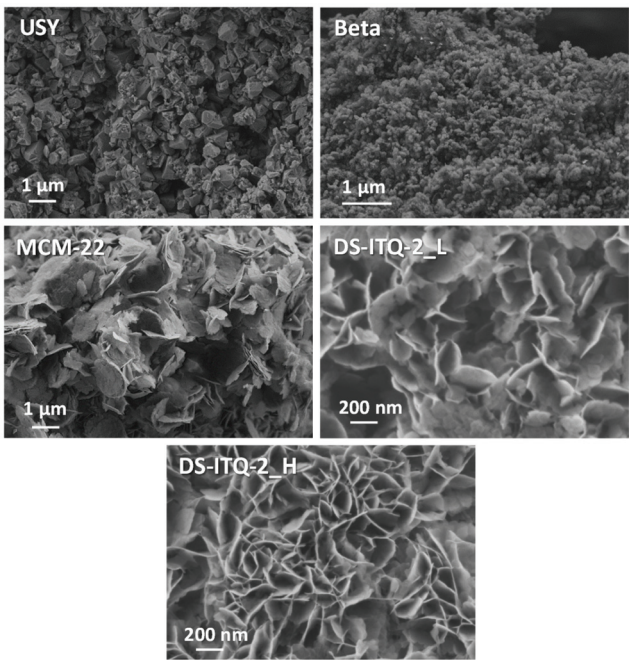

Fig. 4 FE-SEM images of the different zeolites employed in this study.

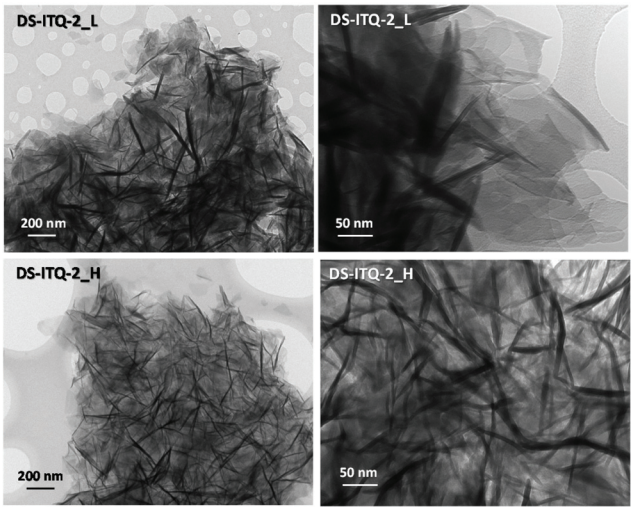

Fig. 5 HRTEM images of the DS-ITQ-2_L (top) and DS-ITQ-2_H (bottom) samples at different magnifications.

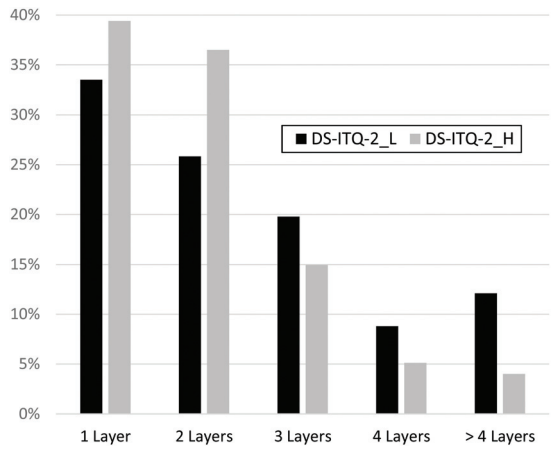

Fig. 6 Crystallite distribution of DS-ITQ-2 samples according to the number of layers.

The textural properties of these delaminated DS-ITQ-2 materials have been measured by N_2 adsorption characterization. As seen in Fig. 7, the N_2 adsorption isotherms of the ITQ-2 type materials, DS-ITQ-2_L and DS-ITQ-2_H, show a considerably higher N_2 adsorption uptake at higher relative pressures ($P/P_0 > 0.9$) compared to the other zeolites, suggesting that these ITQ-2 type materials would favor interparticle condensation at these higher relative pressures as a consequence of their highly delaminated nature. The measured external surface areas for DS-ITQ-2_H and DS-ITQ-2_L are 214 and 146 $m^2\ g^{-1}$, respectively (see Table 1), in good agreement with the observed slopes and overall N_2 uptakes in the N_2 adsorption isotherms at intermediate and high relative pressures (see Table 1 and Fig. 7). This characterization suggests that the DS-ITQ-2_H sample will provide a larger proportion of external surface hemicavities or "cups" than DS-ITQ-2_L, as it could be expected by the higher delaminated nature of the former.

Finally, the measured Si/Al molar ratios by ICP analysis are similar for both samples, Si/Al ~ 11 (see Table 1), which are also comparable to the values introduced in the initial synthesis gels (see the Experimental section). Moreover, the ^{27}Al MAS NMR spectra indicate that almost 80% of these Al species remain in tetrahedral coordination for the activated acid form of the catalysts (see signals centered at 50–60 ppm for DS-ITQ-2_L and DS-ITQ-2_H in Fig. 8).

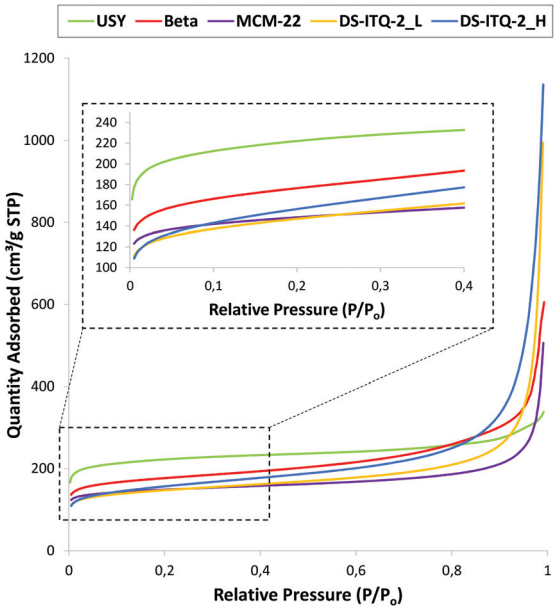

Fig. 7 N_2 adsorption isotherms measured for the studied zeolite materials at 77 K.

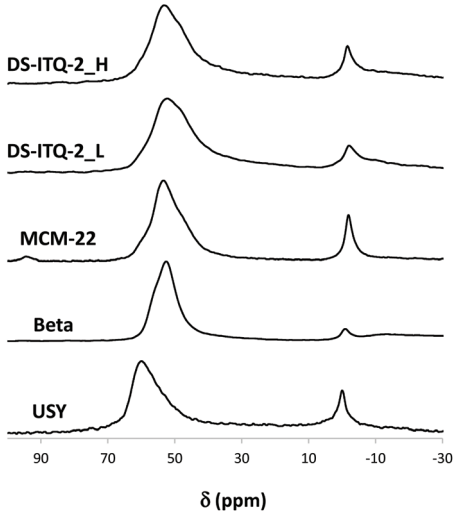

Fig. 8 ^{27}Al MAS NMR of the zeolites in their acid forms.

A standard MCM-22 material with a Si/Al molar ratio of 12 has also been prepared following the procedure reported in the literature (see the Experimental section for details).[34] This material presents the crystalline structure of the MWW framework (see MCM-22 in Fig. 3). The average particle size of the MCM-22 sample is ~0.3–0.5 μm, which is slightly larger than that achieved for the partially delaminated DS-ITQ-2 samples (see FE-SEM images in Fig. 4). N_2 adsorption measurement shows a lower external surface area for the MCM-22 (78 m^2 g^{-1}, see Table 1) accordingly with the crystalline size along the *c*-axes. ICP analysis indicates that the Si/Al molar ratio is analogous to the value introduced in its preparation (~12, see Table 1), with almost 80% of the Al species remaining in tetrahedral coordination in the acid-form sample (see signals centered at 50–60 ppm for the ^{27}Al MAS NMR spectra of MMCM-22 in Fig. 8).

3.3. Catalytic activity for conversion of biomass-derived DMF to *p*-xylene

The reaction of DMF with ethylene using the above-described catalysts has been carried out at 52 bar and 240 °C with heptane as the solvent (see details in the Experimental section). In addition to the MWW-type materials, two commercially available Beta (BEA) and USY (FAU) zeolites have also been selected for comparison purposes (see the Experimental section for details).

After 3 hours of reaction, the two one-pot synthesized DS-ITQ-2 samples present the best catalytic activities, reaching DMF conversion values of 44.2 and 36.5% for the high-delaminated DS-ITQ-2_H and low-delaminated DS-ITQ-2_L, respectively (see Fig. 9a). The catalytic activities of the two DS-ITQ-2 zeolites are significantly higher than the values observed for the two-commercial zeolites selected for comparison purposes, where USY and Beta zeolites are able to convert 17.8 and 26.3%, respectively (see Fig. 9a). The rank of zeolite activity is in good agreement with the DFT calculations, where the host–guest confinement interactions calculated for the DA cycloadduct within the micropores are higher in Beta than in FAU, and much higher in the case of DS-ITQ-2. Interestingly, the enhanced DMF conversion values observed for the high-delaminated DS-ITQ-2_H and low-delaminated DS-ITQ-2_L zeolites are maintained at longer reaction times (77.7 and 64.4%, respectively, after 20 h of reaction, see Fig. 9b) compared to Beta and USY (44.6 and 31.8%, respectively, see Fig. 9b).

In addition, when the catalytic activity of the MWW-type materials is compared, large differences can clearly be observed (see Fig. 9a). The standard MCM-22 zeolite shows a DMF conversion value of ~18% after 3 hours of reaction, which is lower than the values achieved when using the two one-pot synthesized delaminated DS-ITQ-2 materials (see

Table 1 Physicochemical properties of the different zeolites

Sample	Si/Al	BET suf. area (m^2 g^{-1})	External surf. area (m^2 g^{-1})	Microp. area (m^2 g^{-1})	Microp. Vol. (cm^3 g^{-1})
USY	14.0	600	66	534	0.27
Beta	11.8	532	186	346	0.17
MCM-22	12.3	507	78	429	0.20
DS-ITQ-2_L	10.9	546	146	400	0.16
DS-ITQ-2_H	11.6	566	214	352	0.15

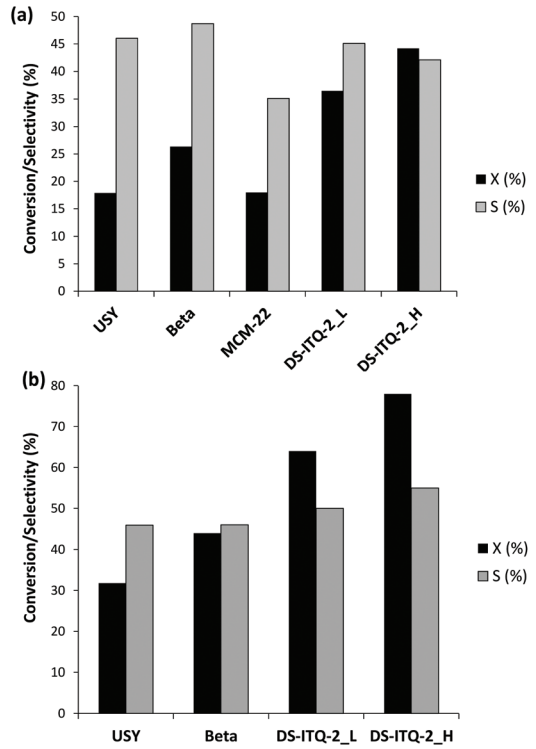

Fig. 9 Dimethylfuran (DMF) conversion and *p*-xylene selectivity for the Diels–Alder dehydration reaction between DMF and ethylene after 3 h (a) and 20 h (b). Reaction conditions: 14.6 mmol DMF, 28.1 ml heptane and 30 mg of catalyst, at 52 bar and 240 °C.

Fig. 9a). Interestingly, the representation of the TOF of these three materials after 3 h of reaction, calculated as mmol converted of DMF per mmol of Al in tetrahedral coordination within these materials, *versus* their measured external surface area by N_2 adsorption, follows a quasi linear trend, as it can be clearly observed in Fig. 10 (see MCM-22, DS-ITQ-2_L and DS-ITQ-2_H). Therefore, the good correlation between the external surface area of these three materials and the catalytic activity would be mostly attributed to the increase of accessible external "cups" able to undergo the DA reaction. It is worth noting that the dual benefits of the DS-ITQ-2_H catalyst are that it combines the right cavity confinement with high accessibility from the external surface area. Indeed, a nanosized Beta zeolite (CP811, Zeolyst) with practically the same accessible external surface area (186 $m^2\ g^{-1}$) as the two-dimensional DS-ITQ-2 zeolites gives much lower DMF conversion (see Fig. 9).

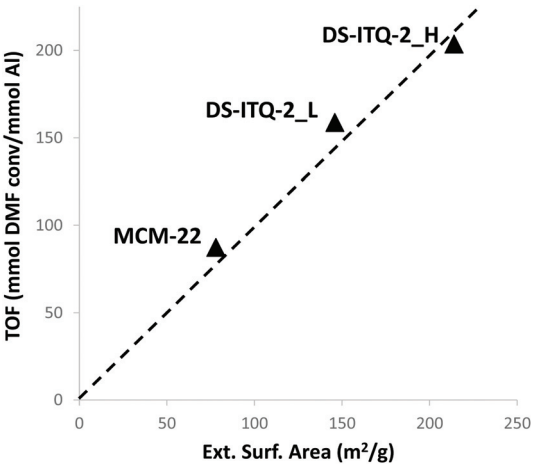

Fig. 10 TOF (mmol DMF converted per mmol Al) after 3 h for the Diels–Alder dehydration reaction using dimethylfuran (DMF) and ethylene front the external surface area of the different MWW-type materials.

The product selectivity towards *p*-xylene ranges between 45 and 50% for the zeolite catalysts after 3 hours of reaction (see Fig. 9a). It has been proposed that the Brønsted acidity associated with Al-containing zeolites could be responsible not only for the required dehydration of the intermediate cycloadduct towards the *p*-xylene (see Fig. 1), but also for catalysing the formation of other unwanted alkylated products or condensed products.[4,14,15] Indeed, when analysing the presence of other by-products in the reaction mixtures of the different catalysts (see the typical GC chromatogram in Fig. S2†), similar presence of condensed products, for instance those achieved from the interaction between DMF and the intermediate species involved in the dehydration of oxanorbornene to *p*-xylene,[8] is observed (see Table S1†). Considering that some authors have described that increasing the Si/Al molar ratios or incorporating Lewis acid sites could help to increase the *p*-xylene selectivity, since weak acidities would prevent the formation of undesired polymerized or alkylated products,[4,14,15] current efforts in our group focus on attempting the synthesis of the DS-ITQ-2 with different chemical compositions to evaluate the further impact on product selectivity.

4. Conclusions

Periodic DFT calculations have allowed evaluation of the stabilization by confinement of the intermediate DA cycloadduct proposed for the tandem DA cycloaddition/dehydration of biomass-derived dimethylfuran and ethylene to achieve *p*-xylene within different zeolitic structures, including FAU, Beta and MWW. This theoretical study has shown a very important confinement stabilization of the intermediate DA cycloadduct in the external surface "cups" of the MWW structure (−19.6 kcal mol^{-1}), which exceeds the calculated host–guest interactions in other zeolite frameworks (−12.0 and −15.7 kcal mol^{-1} for FAU and BEA, respectively). Diverse MWW-type zeolites have been prepared with different textural properties, including the classical MCM-22 zeolite, and delaminated DS-ITQ-2 materials with diverse delamination degrees. The delaminated DS-ITQ-2 materials give enhanced reaction rates compared to other zeolite structures (Beta and FAU), in good agreement with DFT calculations. These preliminary results undoubtedly reveal the excellent role of the external MWW "cups" as reaction-adapted sites to efficiently perform the biomass-derived cycloaddition reaction. This work

is a very interesting example demonstrating how "*ab initio*" DFT predictions can assist the selection and design of a particular zeolite catalyst with adequate physico-chemical properties to enhance the catalytic performance for a target chemical process.

Conflicts of interest

There are no conflicts to declare.

Acknowledgements

This work has been supported by the European Union through ERC-AdG-2014-671093 (SynCatMatch) and by Spanish Government through "Severo Ochoa" (SEV-2016-0683, MINECO), MAT2017-82288-C2-1-P (AEI/FEDER, UE) and RTI2018-101033-B-I00 (MCIU/AEI/FEDER, UE). E. M. G. acknowledges "La Caixa – Severo Ochoa" International PhD Fellowships (call 2015). Elisa García is acknowledged for her technical assistance in this work. The Electron Microscopy Service of the UPV is also acknowledged for their help in sample characterization. We appreciate the support of ExxonMobil Research and Engineering for their help with our efforts in fundamental catalytic research.

Notes and references

1 P. A. Owusu and S. Asumadu-Sarkodie, *Cogent Eng.*, 2016, **203**, 1167990.
2 A. Corma, S. Iborra and A. Velty, *Chem. Rev.*, 2007, **107**, 2411–2502.
3 A. Settle, L. Berstis, N. Rorrer, Y. Roman-Leshkov, G. Beckham, R. Richards and D. Vardon, *Green Chem.*, 2017, **19**, 3468–3492.
4 C. L. Williams, C. C. Chang, P. Do, N. Nikbin, S. Caratzoulas, D. G. Vlachos, R. F. Lobo, W. Fan and P. J. Dauenhauer, *ACS Catal.*, 2012, **2**, 935–939.
5 J. J. Pacheco and M. E. Davis, *Proc. Natl. Acad. Sci. U. S. A.*, 2014, **111**, 8363–8367.
6 R. A. F. Tomás, J. C. M. Bordado and J. F. P. Gomes, *Chem. Rev.*, 2013, **113**, 7421–7469.
7 Y. C. Lin and G. W. Huber, *Energy Environ. Sci.*, 2009, **2**, 68–80.
8 P. T. M. Do, J. R. McAtee, D. A. Watson and R. F. Lobo, *ACS Catal.*, 2013, **3**, 41–46.
9 J. B. Binder and R. T. Raines, *J. Am. Chem. Soc.*, 2009, **131**, 1979–1985.
10 M. FitzPatrick, P. Champagne, M. F. Cunningham and R. A. Whitney, *Bioresour. Technol.*, 2010, **101**, 8915–8922.
11 R. Y. Rohling, I. C. Tranca, E. J. M. Hensen and E. A. Pidko, *J. Phys. Chem. C*, 2018, **122**, 14733–14743.
12 R. Y. Rohling, E. Uslamin, B. Zijlstra, I. C. Tranca, I. A. W. Filot, E. J. M. Hensen and E. A. Pidko, *ACS Catal.*, 2018, **8**, 760–769.
13 T. W. Kim, S. Y. Kim, J. C. Kim, Y. Kim, R. Ryoo and C. U. Kim, *Appl. Catal., B*, 2016, **185**, 100–109.
14 C. C. Chang, H. J. Cho, J. Yu, R. J. Gorte, J. Gulbinski, P. Dauenhauer and W. Fan, *Green Chem.*, 2016, **18**, 1368–1376.
15 H. J. Cho, L. Ren, V. Vattipalli, Y. H. Yeh, N. Gould, B. Xu, R. J. Gorte, R. Lobo, P. J. Dauenhauer, M. Tsapatsis and W. Fan, *ChemCatChem*, 2017, **9**, 398–402.
16 R. Zhao, Z. Zhao, S. Li, A. N. Parvulescu, U. Muller and W. Zhang, *ChemSusChem*, 2018, **11**, 3803–3811.
17 C. C. Chang, S. K. Green, C. L. Williams, P. J. Dauenhauer and W. Fan, *Green Chem.*, 2014, **16**, 585–588.
18 Y. P. Li, M. Head-Gordon and A. T. Bell, *J. Phys. Chem. C*, 2014, **118**, 22090–22095.
19 N. Nikbin, S. Feng, S. Caratzoulas and D. G. Vlachos, *J. Phys. Chem. C*, 2014, **118**, 24415–24424.
20 R. Y. Rohling, E. J. M. Hensen and E. A. Pidko, *ChemPhysChem*, 2018, **19**, 446–458.
21 E. G. Derouane, J. M. Andre and A. A. Lucas, *J. Catal.*, 1988, **110**, 58–73.
22 A. Corma, *Catal. Rev.*, 2004, **46**, 369–417.
23 R. Gounder and E. Iglesia, *Chem. Commun.*, 2013, **49**, 3491–3509.
24 F. Marquez, H. Garcia, E. Palomares, L. Fernández and A. Corma, *J. Am. Chem. Soc.*, 2000, **122**, 6520–6521.
25 A. Bhan, A. D. Allian, G. J. Sunley, D. J. Law and E. Iglesia, *J. Am. Chem. Soc.*, 2007, **129**, 4919–4924.
26 A. Bhan and E. Iglesia, *Acc. Chem. Res.*, 2008, **41**, 559–567.
27 M. Boronat, C. Martinez-Sanchez, D. Law and A. Corma, *J. Am. Chem. Soc.*, 2008, **130**, 16316–16323.
28 E. M. Gallego, M. T. Portilla, C. Paris, A. León-Escamilla, M. Boronat, M. Moliner and A. Corma, *Science*, 2017, **355**, 1051–1054.
29 C. Li, C. Paris, J. Martinez-Triguero, M. Boronat, M. Moliner and A. Corma, *Nat. Catal.*, 2018, **1**, 547–554.
30 R. M. Dessau, *J. Chem. Soc., Chem. Commun.*, 1986, 1167–1168.
31 E. M. Gallego, C. Paris, A. Cantín, M. Moliner and A. Corma, *Chem. Sci.*, 2019, **10**, 8009–8015.
32 V. J. Margarit, M. E. Martínez-Armero, M. T. Navarro, C. Martínez and A. Corma, *Angew. Chem., Int. Ed.*, 2015, **54**, 13724–13728.
33 M. E. Leonowicz, J. A. Lawton, S. L. Lawton and M. K. Rubin, *Science*, 1994, **264**, 1910–1913.
34 A. Corma, C. Corell and J. Pérez-Pariente, *Zeolites*, 1995, **15**, 2–8.
35 H. K. Min and S. B. Hong, *J. Phys. Chem. C*, 2011, **115**, 16124–16133.
36 S. Laforge, D. Martin and M. Guisnet, *Appl. Catal., A*, 2004, **268**, 33–41.
37 A. Corma, V. Fornes, S. B. Pergher, T. Maesen and J. G. Buglass, *Nature*, 1998, **396**, 353–356.
38 G. Kresse and J. Furthmüller, *Phys. Rev. B: Condens. Matter Mater. Phys.*, 1996, **54**, 11169–11186.
39 J. P. Perdew, K. Burke and M. Ernzerhof, *Phys. Rev. Lett.*, 1996, **77**, 3865–3868.

40 J. P. Perdew, K. Burke and M. Ernzerhof, *Phys. Rev. Lett.*, 1997, **78**, 1396–1398.
41 S. Grimme, *J. Comput. Chem.*, 2006, **27**, 1787–1799.
42 P. E. Blöchl, *Phys. Rev. B: Condens. Matter Mater. Phys.*, 1994, **50**, 17953–17979.
43 G. Kresse and D. Joubert, *Phys. Rev. B: Condens. Matter Mater. Phys.*, 1999, **59**, 1758–1775.